A Quantum Chemical Approach to the Influence of Platinum Surface Structure on the Oxygen Electroreduction Reaction

C. F. Zinola and A. J. Arvia*

Instituto de Investigaciones Fisicoquímicas Teóricas y Aplicadas (INIFTA), Universidad Nacional de La Plata, Sucursal 4, Casilla de Correo 16, (1900) La Plata, Argentina

G. L. Estiu and E. A. Castro

Programa de Química Inorgánica (QUINOR), Universidad Nacional de La Plata, Casilla de Correo 962, (1900) La Plata, Argentina

Received: January 21, 1994; In Final Form: May 2, 1994®

The O_2 electroreduction reaction (OERR) on Pt behaves as a structure sensitive reaction whose peroxo intermediates are formed in a greater extent on Pt(100) than on Pt(111) surfaces. A semiempirical quantum chemistry interpretation of this behavior is attempted on the basis of the study of $[Pt]_NO_2OH$ systems, where N, the number of atoms in the Pt cluster, equals 18 and 25. Calculations indicate that dissociative O_2 electroadsorption on Pt(111) and molecular O_2 on Pt(100) are favored. As a result of the interactions of O_2 and OH in adjacent positions, hydroperoxide intermediates are formed on Pt(100) leading to the possibility of having H_2O_2 as product from the OERR.

1. Introduction

The molecular oxygen electroreduction reaction (OERR) on Pt in acid solutions is one of the most relevant electrochemical reactions.[1-3] It has been interpreted by a complex mechanism involving first the adsorption of molecular O_2, followed by a charge-transfer step and desorption of electroreduced adsorbates, finally leading to H_2O as the main product, and to H_2O_2 as minor product.[4-6]

Recent OERR kinetic data have shown different current density vs electrode potential relationships, depending on the topography of the Pt electrode in both acid[7,8] and alkaline solutions.[9] To account for these results,[6,10-12] a more adequate interpretation of the OERR kinetics can be given by considering that there is a competition between the four-electron electroreduction to H_2O and the two-electron electroreduction to H_2O_2, which can further decompose to H_2O. The relative contribution of each reaction depends on the Pt surface crystallography, the applied potential, and the nature and concentration of anions in the solution.[13,14] The value of θ_o, the stationary Pt surface coverage by O-containing adsorbates in O_2-saturated solution, changes almost linearly with the applied potential for all Pt surfaces.[7] However, values of θ_o are greater for Pt(100) than for Pt(111) and polycrystalline (pc) Pt, implying for the former an additional contribution to θ_o from other oxygenated adsorbed species.

The formation of H_2O_2 in the course of the OERR in aqueous solutions was almost twice as much for Pt(100) than for Pt(111) and pc Pt electrodes.[7] The difference indicates either a more strongly adsorbed peroxide species or a faster H_2O_2 decomposition on Pt(111) and pc Pt surfaces. Furthermore, the higher contribution of peroxo intermediates to the OERR on Pt(100) can explain the greater θ_o values found in O_2-saturated acid solutions.[7]

The difference in the electronic characteristics of adsorption sites, resulting from the different crystallographic structures, leads to a topology dependence of the heterogeneous catalytic reaction kinetics. It has recently been found for the OERR on faceted[7,9] and single crystal[8] Pt electrodes that there is a structure sensitivity in both acid and alkaline media, with a larger relative contribution of the two-electron reaction pathway on Pt(100) than on Pt(111) and pc Pt. There facts were assigned to different interactions between O_2 and the reaction intermediates with Pt(100) and Pt(111) surface structures.

Both experimental gas-phase[15-18] and theoretical[19-24] studies have shown different characteristics of O_2 adsorption on Me(100) and Me(111) surfaces (Me = transition metal). Thus, adsorbate configurations, resulting from molecular O_2 adsorption on Pt(100) (5×20) surfaces, depend on the degree of reconstruction of the Pt surface, as it can be inferred from thermal desorption spectroscopy (TDS) and X-ray photoemission measurements.[25] Activation energies of ca. 0.4 eV were found by molecular beam studies[15] for the dissociative adsorption of O_2 on Pt(100) with an enhancement of the sticking probability and no change on the threshold dissociation energy between 300 and 600 K.

Otherwise, on Pt(111), molecular O_2 only predominates with respect to the O adatom, at temperatures below 120 K.[26] Electron energy loss spectroscopy (EELS) data show a primary vibrational mode at 870 cm^{-1}, which is characteristic of peroxo-type species.[26,27] According to near edge X-ray adsorption fine structure studies (NEXAFS),[28-31] molecular O_2 lies with the intermolecular axis parallel to the metal surface, in agreement with EELS detection of peroxo species. Likewise, O adatoms predominant at temperatures higher than 170 K, since a single vibrational mode at 490 cm^{-1}, attributed to the O–Pt stretching frequency, is detected.[26,32] Hence, the different behavior of the O_2(gas)/Pt(111) and O_2(gas)/Pt(100) systems provides a first indication of different surface structure O_2–Pt interactions which, in principle, could be reflected to some extent in the OERR on different Pt substrates.

Theoretical calculations are mainly related to lower-atomic-number transition metals.[19-21,23,24] To our knowledge, no previous theoretical study of the Pt_NO_2 system has involved either the optimization of the adsorbate structure or the influence of the applied potential.

In this paper, the interaction of an O_2 molecule with Pt(100) and Pt(111) cluster surfaces is analyzed at a molecular orbital level, as a first step to understand the influence of the electrode topology on the OERR mechanism. In this way, the selective generation of peroxo species on Pt(100) can be justified on the basis of the involved molecular orbital interactions and the different nature of the adsorbed intermediates on both surfaces.

® Abstract published in *Advance ACS Abstracts*, June 15, 1994.

0022-3654/94/2098-7566$04.50/0

2. Methodology

2.1. Calculation Procedure. For the treatment of large polyatomic systems, computational chemistry deals, nowadays, with a compromise between an overall description of the entire system and a more detailed treatment of a properly selected part of it. This situation particularly applies to transition metal structures, which have to be drastically minimized for an adequate ab initio, local density functional, or even semiempirical calculation at a good correlation level.[33-36] In contrast to this simplification of the system, the improvement of simpler methods, which are capable of handling the system as a whole, have regained acceptability. This is the case of the extended Hückel molecular orbital (EHMO) method developed by Hoffman,[37] which was initially used for a reasonable description of the structural and electronic properties of systems at a frozen geometry. Improvements of this method are mainly related to the addition of two-body electrostatic correction terms.[38-42] Accordingly, E_T, the total energy of the system, is calculated from the contribution of two terms:

$$E_T = \Delta E_{EHMO} + E_{rep} \quad (1)$$

$$\Delta E_{EHMO} = E_{EHMO} - \sum_{\mu} b_\mu^\circ E_\mu^\circ \quad (2)$$

where ΔE_{EHMO} is the EHMO binding energy, calculated as the difference between E_{EHMO}, the noncorrected EHMO total energy and the summation of the monoelectronic terms; b_μ° and E_μ° are the occupation number and the valence state ionization potential (VSIP) of the μth atomic orbital. The correction implies the addition of E_{rep}, the repulsion energy,

$$E_{rep} = \sum_{A} \sum_{B<A} E_{AB} \quad (3)$$

where E_{AB} is the electrostatic repulsion energy between atoms A and B separated by the distance R_{AB}. E_{rep} is a pairwise additive term which can be either explicitly calculated for a given pair of atoms[38,39,42] or determined from binding energy differences when inner orbitals are either considered or neglected.[40,41]

Calzaferri et al.[42-46] have reformulated the EHMO method by including the following two main modifications.

i. A repulsion energy that explicitly considers both atoms of a given pair,

$$E_{AB} = \frac{Z_A Z_B}{R_{AB}} - {}^1/_2 \left[Z_A \int \frac{\rho_B(\bar{r})}{|\bar{R}_A - \bar{r}|} d\bar{r} + Z_B \int \frac{\rho_A(\bar{r})}{|\bar{R}_B - \bar{r}|} d\bar{r} \right] \quad (4)$$

where Z_i, $\bar{R}_i$ and ρ_i are the nuclear charge, position, and electron density of atom i, (i = A, B), where atom B is more electronegative than atom A. The second right-hand side term in eq 4 is the arithmetic mean of A–B and B–A attractive interaction energies.

ii. A distance-dependent exponential factor that modifies the off-diagonal EHMO matrix elements according to

$$H_{\mu\nu}^{AB} = \frac{1}{2} K_{AB} (H_{\mu\mu} + H_{\nu\nu}) S_{\mu\nu} \quad (5)$$

where K_{AB} and δ are adjustable parameters related by the expression

$$K_{AB} = 1 + \kappa \exp[-\delta (R_{AB} - d_0)] \quad (6)$$

K_{AB} is the EHMO-K parameter used in the off-diagonal Hamiltonian matrix elements, $H_{\mu\nu}^{AB}$, μ and ν being the μth and the νth orbitals of atoms A and B, respectively. d_0 is the sum of the atomic radii of A and B. K_{AB} and δ are empirical parameters, such as $1.4 \le (1 + \kappa) \le 2.5$ and $0.0 \le \delta \le 0.1$ nm^{-1}. The other energy matrix elements are kept as given by the conventional EHMO methodology, *i.e.*

$$H_{\mu\mu}^{AA} = -(VSIP)_\mu^A; \quad H_{\mu\nu}^{AA} = 0 \quad (7a,b)$$

It has been demonstrated that a careful parametrization of the reformulated EHMO method allows us to optimize the geometry of either simple[42-46] or organometallic complex molecules[43] at a level that can be compared with high-quality calculations.

The preceding calculation procedure was employed to analyze the interaction of a single O_2 molecule with Pt(111) and Pt(100) cluster surfaces, including the influence of an applied electrical potential. Because of the complex nature of the electrochemical interface, which involves the solution constituents, adsorbates, and substrate, the interaction energy resulting from coadsorbed species was considered to find out whether O_2 dissociation is favored and to envisage the stability of adsorbates and final products, which can be related to the OERR on different Pt electrode surfaces.

2.2. Calculation Details. Values of the VSIP in eq 5 are experimentally based, and valence orbitals are of the Slater form. The O_2 molecule–Pt site interactions are represented as an adsorbed ensemble, which is characterized by its specific VSIP. The VSIP value, which defines the equilibrium potential of the system, *i.e.*, the zero applied potential condition, results when the charge transfer at the equilibrium distance of each internuclear bond is close to that predicted for the adsorbed ensemble from the electronegativity difference, according to Pauling's ionicity relationship.[53] VSIP values, adjusted in this way, are assembled in Table 1.

TABLE 1: Optimized Parameters from EHMO Calculations

orbital	VSIP[a]/eV	ζ_1[b]	ζ_2[b]	c_1[c]	c_2[c]
Pt 5d	−12.83	4.0950	1.8600	0.7980	0.3520
Pt 6s	−9.32	1.9830			
Pt 6p	−5.72	1.3440			
O 2s	−27.96	2.5640			
O 2p	−12.16	2.2640			
H 1s	−13.30	1.3000			

[a] VSIP ≡ valence state ionization potential. [b] $\zeta_{1,2}$ ≡ exponents of the base generating functions. [c] $c_{1,2}$ ≡ coefficients of the double ζ Pt d orbitals.

Following the previously described method,[54] VSIP and Slater orbital exponents were taken from refs 46 and 54 for the substrate and the adsorbate, respectively. Values δ = 0.035 nm^{-1} and K_{AB} = 1.75 have been set in eq 6. Results from different K_{AB} values ($1.5 \le K_{AB} \le 2.0$) have also been compared, and the K_{AB} that best describes bond lengths and adsorption energies in Pt_5 *testing clusters* has been adopted. The VSIP adjustment to charge-transfer conditions was made for different (K,δ) pairs. The best set of K, δ, VSIP, and Slater orbitals was finally chosen from the description of the adsorption interactions.

As a positive applied electric potential (E) shifts downward the metal energy Fermi level and vice versa, changes in the electrode potential were simulated by either decreasing or increasing the absolute value of the metal VSIP from the reference equilibrium value, for negative or positive charging, respectively[55,56] (Table 1). The Δ(VSIP)/ΔE value was set equal to 1, as there was no other clear experimental evidence which could justify a different choice.

High spin bulk superimposable bilayer Pt_N clusters, with the number of atoms N = 18 and N = 25 for Pt(100), and N = 18 for Pt(111), (Figure 1), were used to model Pt surfaces. Clusters were geometrically built up, keeping the Pt–Pt bond length, r_{Pt-Pt}, constant at 0.277 nm. This figure, which has been used in previous calculations,[55,56] agrees with the Pt–Pt interatomic distance in bulk Pt.[57] The open shell configuration of the O_2 molecule ($^3\Sigma_g^-$) has been considered in the definition of the spin magnetic

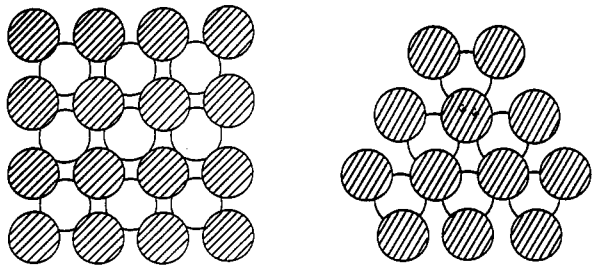

Figure 1. Clusters used to model (a) Pt(100) and (b) Pt(111) surfaces.

moment of the Pt_NO_2 adsorbed ensemble which, according to the d-rule,[58] involves at least one electron in each d-band molecular orbital.

Different types of adsorption sites can be defined on Pt single crystals, namely, on-top (1-fold), bridge (2-fold), and hollow (higher coordinated sites). Hollow sites are associated with a 5-fold coordination of an O atom on Pt(100) (four Pt atoms of the topmost layer and one Pt atom from the underlying layer). Otherwise, either three or four Pt atoms may define the hollow coordination in Pt(111), depending on whether the fcc or the hcp local symmetry, *i.e.*, the (3–1) or the (3–3) hollow site, respectively, is involved. The interaction of an O_2 molecule with these sites defines several adsorption configurations (see section 3.1).

The interaction of a single O_2 molecule with a Pt surface was initially considered, but the OERR in aqueous environments also involves H_2O and other coadsorbed intermediates on the Pt surface. In the 0.60–1.00-V (vs reversible hydrogen electrode) potential range, where O_2 adsorption takes place, there is an important contribution of adsorbed OH species. Therefore, the stability of the adsorbed ensemble, constituted by O_2, OH, and Pt sites, was evaluated as a function of the applied potential. While the coordinates of the Pt atoms were kept frozen in the calculations, the Pt–O, O–O, and O–H distances and angles were fully optimized to minimum energy.

3. Results and Interpretation

3.1. Interaction of a Single O_2 Molecule with Pt(111) and Pt(100) Cluster Surfaces: The Most Likely Stable Configuration of the Adsorbed Pt_NO_2 Ensemble. Because of the important role of O_2 frontier orbitals (π, π^*) in the interaction with the Pt surface, adsorption geometries with the O–O interatomic bond parallel to the Pt surface plane are likely to occur. However, the "parallel" (side-on) and the "perpendicular" (end-on) configurations were compared. Among possible configurations, the most important ones are those which involve either the coordination of one O atom to a single surface site (1-fold, bridge and hollow coordination) (Figure 2a–c) or the simultaneous coordination of both O atoms from O_2 to a unique surface site (on-top side-on or bridge side-on configuration) (Figure 2d,e).

The geometry of each adsorbate configuration was fully optimized in bond distances and planar and dihedral angles, taking into account the orientation of the O–O bond relative to the Pt–Pt bond in the lattice.

The geometrical characteristics and relative stabilities of each adsorbate structure are compared in Table 2. Binding energies, BE, were calculated as

$$\mathrm{BE} = -(E_{\mathrm{T},\mathrm{Pt}_N\mathrm{O}_2} - E_{\mathrm{T},\mathrm{Pt}_N} - E_{\mathrm{T},\mathrm{O}_2}) \qquad (8)$$

where $E_{\mathrm{T},\mathrm{Pt}_N\mathrm{O}_2}$, $E_{\mathrm{T},\mathrm{Pt}_N}$, and $E_{\mathrm{T},\mathrm{O}_2}$ are the total energy, of Pt_NO_2, Pt_N, and O_2, respectively, resulting from eq 1. The $E_{\mathrm{T},\mathrm{O}_2}$ value results from a full optimization of the $^3\Sigma_g^-$ configuration, which is known to be the most stable one. From these calculations, r_{O-O}, the equilibrium O–O bond length in an isolated O_2 molecule, = 0.133 nm, a figure which is 6% greater than the experimental

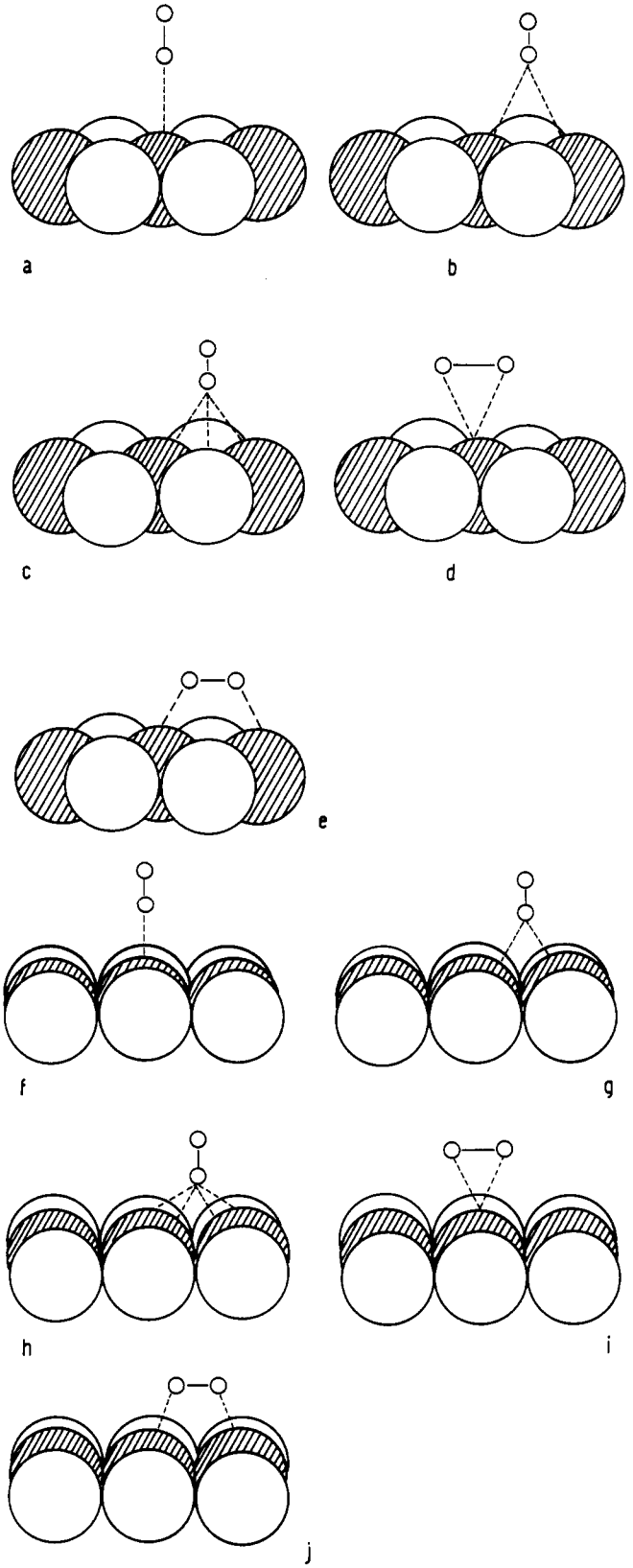

Figure 2. Different Pt_NO_2 adsorption configurations on Pt(100) and Pt(111) surfaces: (a,f) on-top end-on, (b,g) bridge end-on, (c,h) bridge side-on, (d,i) on-top side-on, and (e,j) hollow.

r_{O-O} value,[59,60] and a dissociation energy of 2.02 eV was also calculated. The reproducibility of diatomic O_2 experimental data was also considered for the parameter selection.

The optimization of the adsorbed ensemble geometries implies the simultaneous modification of r_{O-O} and r_{Pt-O}, O–O and Pt–O bond lengths, respectively, Pt–O–O and Pt–Pt–O planar angles, and Pt–Pt–O–O and Pt–Pt–Pt–O dihedral angles. To establish

TABLE 2: Molecular O_2 Binding Energies, BE, Repulsion Energies, RE, Optimized Pt–O and O–O Distances (R_{Pt-O} and r_{O-O}), and Perpendicular Distance from the O Atom Closer to the Plane of the Pt Surface (h), for Different $[Pt(111)]_{18}O_2$ and $[Pt(100)]_{18}O_2$ Configurations at Zero Potential[a]

	BE (eV)	RE (eV)	r_{Pt-O} (nm)	r_{O-O} (nm)	h (nm)
Pt(111)					
on-top end-on	−1.9213	5.5997	0.189	0.120	0.189
bridge end-on	−1.2655	5.5839	0.217	0.116	0.168
bridge side-on	−2.5920	6.2410	0.185	0.138	0.171
on-top side-on	−1.3225	7.9341	0.177	0.258	0.129
hollow (3–1)	0.9211	12.4382	0.167[b]	0.220	−0.006
hollow (3–3)	2.2900	11.3150	0.167[b]	0.220	−0.006
Pt(100)					
on-top end-on	−2.3653	5.5459	0.185	0.120	0.185
bridge end-on	−1.8283	4.8146	0.207	0.130	0.155
bridge side-on	−4.0749	7.3146	0.180	0.119	0.161
on-top side-on	−3.3177	8.5790	0.172	0.243	0.121
hollow	1.5971	7.9083	0.196[b]	0.218	−0.019

[a] For the on-top (side-on) and hollow interactions, BE's correspond to the atomic final state (as can be derived from r_{O-O}). No local minima for the molecular configuration were found. [b] For the hollow configuration, r_{Pt-O} refers to the distance between the deeper O atom and the surface Pt plane.

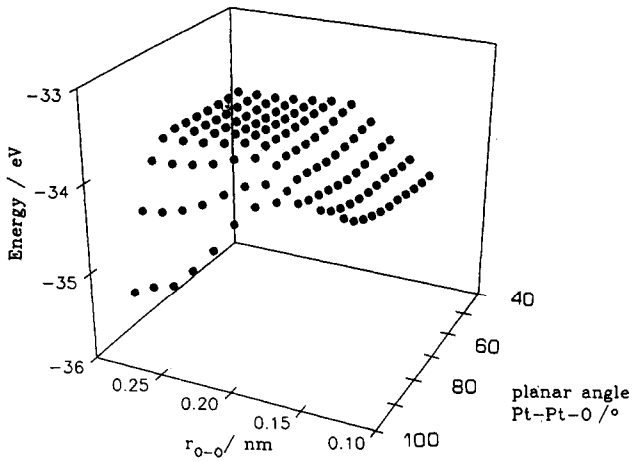

Figure 3. Potential energy hypersurface for the bridge side-on O_2 adsorption configuration on $[Pt(100)]_{18}$ at 0 eV.

whether molecular or dissociative O_2 adsorption takes place, it is convenient to analyze the energy change with r_{O-O} and r_{Pt-O}, that is, through the potential energy hypersurface (Figure 3). This diagram was constructed for each Pt_NO_2 adsorbate ensemble configuration on Pt(111) and Pt(100) clusters, with the simultaneous variations of r_{O-O} and the Pt–Pt–O planar angle (in fact r_{Pt-O}). The most likely reaction pathway for the O_2 dissociation was followed through the minimum energy path in the potential energy profile. For the bridge side-on configuration, the likely pathway for the dissociation process involves first the opening of the planar angle from 64° to 80°, *i.e.*, r_{O-O} from 0.12 to 0.18 nm, then a change in the Pt–O bond length from 0.18 to 0.165 nm, and finally the perpendicular configuration of O atomic species is accomplished. Most of the changes in the potential energy values for the O_2 dissociation are due to the elongation of the O–O bond distance; therefore it is reasonable to admit only r_{O-O} for the definition of the reaction coordinate of the potential energy diagram. For this purpose, 0.001 nm stepwise variations in r_{O-O} were searched for minimum energy from the initial r_{O-O} = 0.080-nm value up to those at which O_2 dissociation occurs. Then, for a fixed r_{O-O} value, other coordinates were fully optimized (Table 2). Optimized geometries correspond to local minima in the energy vs r_{O-O} plot. These minima do not necessarily imply that O_2 dissociation is excluded (Figure 5a,b). As a better description of the potential energy curves for dissociation processes at distances larger than that of equilibrium, the extended Hückel binding energy, BE, can be corrected by means of either a self-consistent charge iteration[44] or the addition of an electrostatic interaction term between the positive and negative species.[61] The stability of the Pt_NO_2 ensemble can be determined from the energy barrier that has to be surmounted to go from molecular O_2 to a single O atom coordinated adsorbate ensemble. According to data shown in Figure 5a,b, local minima in the energy vs r_{O-O} plot are not clearly defined for some configurations, *i.e.*, hollow adsorption on Pt(100) and bridge side-on adsorption on Pt(111). Nevertheless, in these cases, an inflection point in the energy vs r_{O-O} data (unobservable in the energy scale used in the plot) allowed us to calculate the geometric properties of the adsorbates at that point (Table 2).

For the different adsorbate configurations, σ and π O_2 orbitals are involved, their relative weight depending on the specific geometry of the adsorption site.

For the linear on-top end-on coordination (Figure 2a,f) the interaction of the π O_2 molecular orbital with the (d_{xz}, d_{yz}) Pt atomic orbital is more important than that of the σ O_2–d_{z^2} Pt, the z axis being perpendicular to the Pt surface (Figure 4a,f). The contribution of the π^* O_2 molecular orbital to the stability of the d_{xy} Pt atomic orbitals is negligible. The net interaction can be described as a charge transfer to the Pt surface which, being similar for both Pt(111) and Pt(100) (Table 3), reflects the local character of the linear bond.

Otherwise, bridge end-on coordination (Figure 2b,g) implies a greater stabilization of the σ O_2 molecular orbital, through a bonding interaction with adjacent Pt atom $d_{x^2-y^2}$ orbitals, rather than a π-type interaction (Figure 4c,g), which involves a coordination of π orbitals from both Pt and O_2. However, the more important π interaction on Pt(100) than on Pt(111) appears to be responsible for the greater stability of the bridge end-on coordination geometry in Pt(100), and π orbitals are not really hybridized for a further contribution to Pt–Pt bonding. In spite

TABLE 3: Net Charges (q_{O1} and q_{O2}) and σ and π Mulliken Populations in the O Atoms ($MP_\sigma(O_{1,2})$ and $MP_\pi(O_{1,2})$), for Different $[Pt(111)]_{18}O_2$ and $[Pt(100)]_{18}O_2$ Configurations, as Described in Table 2

	q_{O1} (eu)	$MP_\sigma(O_1)$	$MP_\pi(O_1)$	q_{O2} (eu)	$MP_\sigma(O_2)$	$MP_\pi(O_2)$
free O_2	0	3.4737	2.5263	0	3.4737	2.5263
Pt(111)						
on-top end-on	1.5323	2.5353	1.9322	0.7742	2.9175	2.7050
bridge end-on	1.5741	2.4733	1.9525	0.9274	2.9070	2.1654
bridge side-on	0.8598	2.7251	2.4150	0.8598	2.7251	2.4150
on-top side-on	0.7686	2.8708	2.3604	0.7686	2.8708	2.3604
hollow (3–1)	1.6933	2.4457	1.8609	−0.2175	3.2850	2.9324
hollow (3–3)	1.5551	2.4704	1.9743	−0.0626	3.1238	2.9387
Pt(100)						
on-top end-on	1.5204	2.5247	1.9548	0.7075	2.9203	2.3720
bridge end-on	1.4390	2.5284	2.0324	0.5793	2.9562	2.4643
bridge side-on	1.1886	2.6595	2.1517	1.1886	2.6595	2.1517
on-top side-on	0.6294	2.8578	2.5110	0.6294	2.8578	2.5110
hollow	1.6569	2.5687	1.7741	−1.0843	3.7322	3.3520

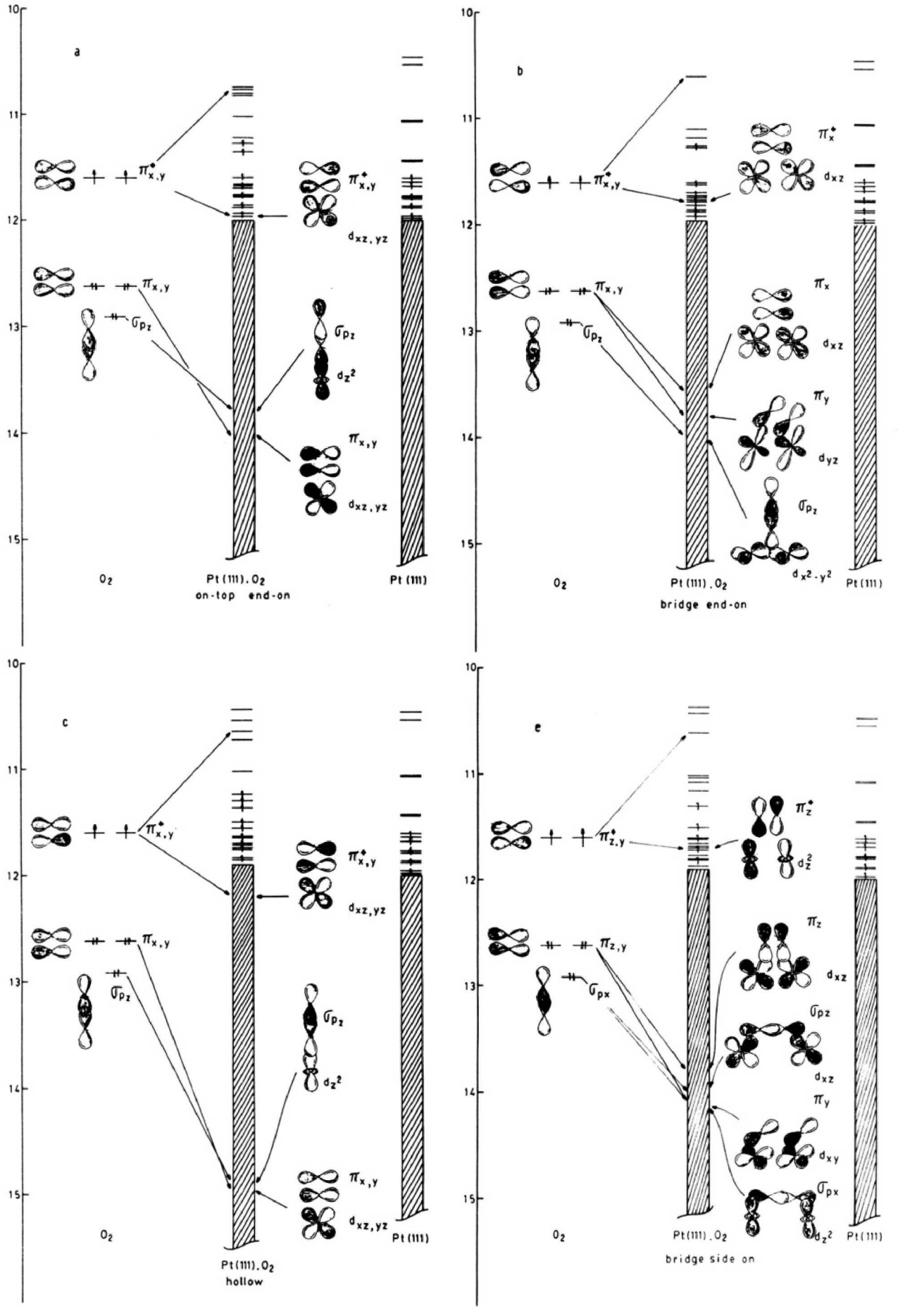
a
b
c
e
O2
Pt(111).O2
on-top end-on
Pt(111)
bridge end-on
hollow
bridge side on
dxz, yz
dz2
dxz
dyz
dxy
dx2-y2

Figure 4

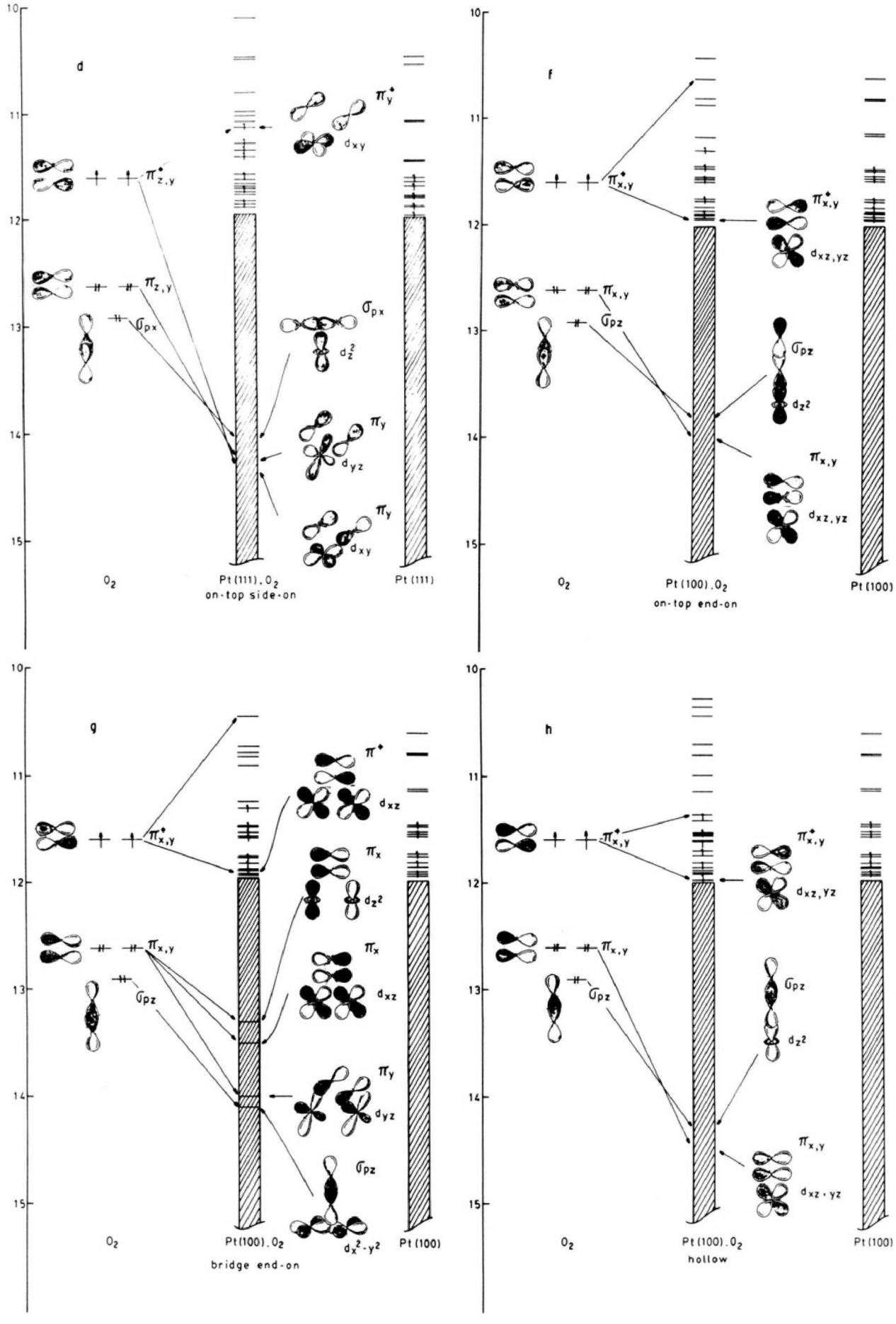

Figure 4 (Continued)

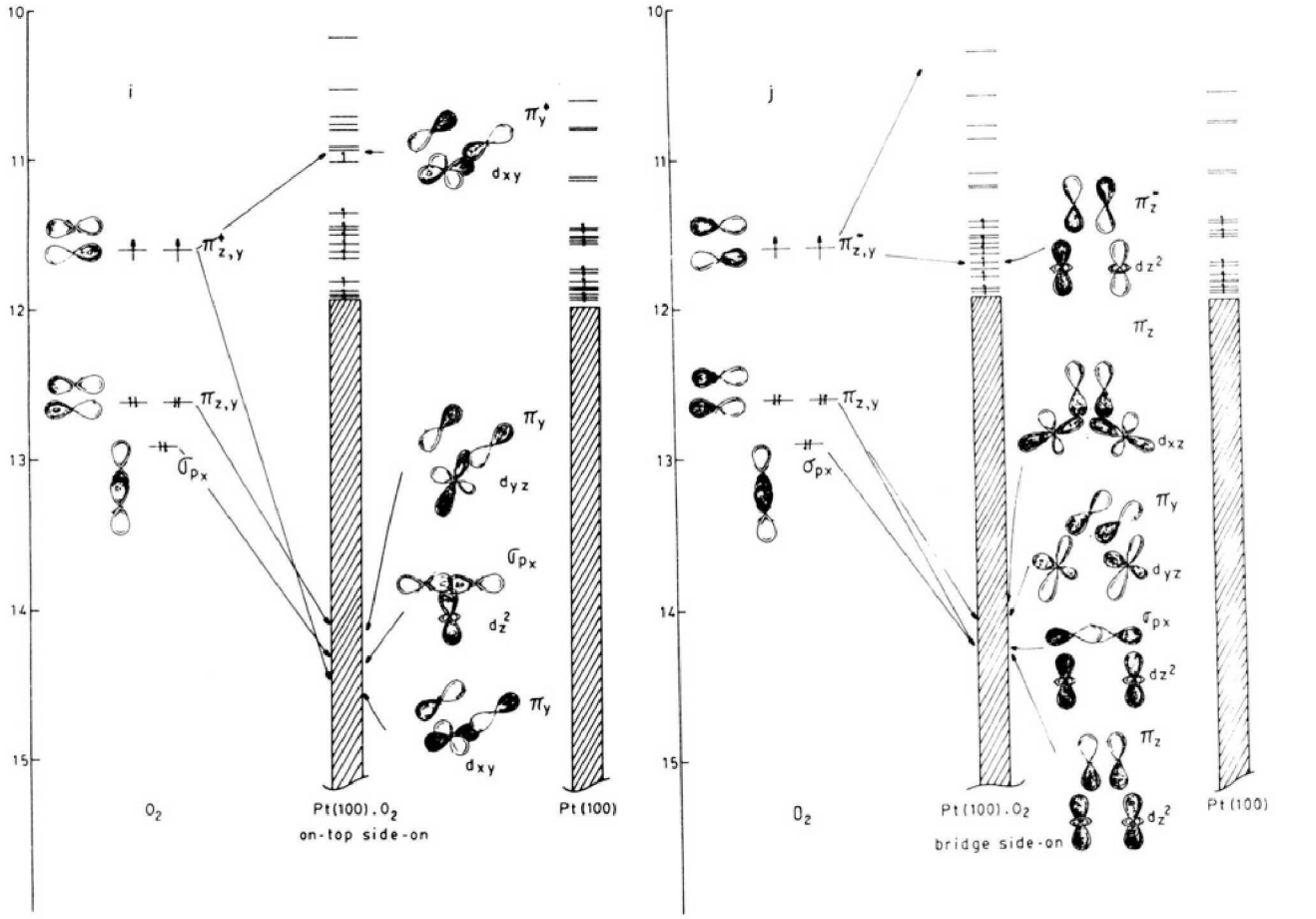

Figure 4. Molecular orbital interaction for different $[Pt(100)]_{18}O_2$ and $[Pt(111)]_{18}O_2$ adsorbate configurations, as depicted in Figure 2: (a,f) on-top end-on, (b,g) bridge end-on, (c,h) hollow, (d,i) on-top side-on, and (e,j) bridge side-on.

of the shorter Pt–O bond length on Pt(100), the lower repulsion energy value (Table 2) is due to the fact that the electron density is lower in the less densely packed Pt(100) structure than in that of Pt(111). The lower repulsion energy value also contributes to the stability of bridge end-on coordinated adsorbate. Both σ and π interactions imply a charge transfer to Pt, as can be inferred from the decrease in σ and π Mulliken populations in O atoms (Table 3). These populations were defined according to the x, y, and z axis contributions to the π and σ orbitals. Unfortunately, no direct comparison of the σ and π relative Mulliken population values of Pt(111) and Pt(100) can be made because the equilibrium geometries to which the data belong are different for both substrates. The greater O–O bond distance (Table 2) for the O_2 molecule adsorbed on Pt(100) agrees with the larger π orbital Mulliken population (Table 3), showing the relevance of the antibonding interactions.

Repulsion energy values become sufficiently large to destabilize hollow adsorption, particularly when a Pt atom and adsorbed O_2 are aligned with the z axis, *i.e.*, hollow Pt(100) and hollow (3–3) in Pt(111) (Table 2, Figure 4c,h). The adsorption bond which results from bonding interactions with a Pt atom in the second layer is similar to that previously described for linear coordination. The most stable configuration on both Pt surfaces implies a nearly dissociated state, which can be simply described as an ionic pair with the positive end closer to the Pt surface. Together with a charge transfer from the O atom closer to the surface, the π Mulliken population in the second O atom increases. Besides, the σ contribution on Pt(100) also increases (Table 3).

On-top side-on adsorbate coordination is characterized by a large stabilization of the π^* O_2 molecular orbital through bonding interaction with d_{xy} Pt atom orbitals, as a consequence of the O_2 adsorbed structure parallel to the surface (Figure 4d,i). The σ and π O_2 molecule bonding orbitals are also involved in this interaction, their relative weights being determined by the specific Pt surface geometry, that is, the O–O bond length. The larger O–O bond length in Pt(111) weakens the σ_p bond in the O_2 molecule and diminishes the importance of the O_2–Pt interaction as compared to Pt(100). Otherwise, the greater O_2 bond length results from a larger π^* orbital population due to a charge transfer from the most densely packed Pt(111) structure. This effect does not reflect in the energy level resulting from the molecular orbital interactions depicted in Figure 4e,j for the bridge side-on geometry, as these interactions involve optimized geometries where interatomic distances are already stabilized, yielding a greater r_{O-O} on Pt(111) resulting from the larger population of the π^* orbitals. As previously discussed for hollow coordination, the r_{O-O} equilibrium value for the on-top side-on adsorbate coordination almost corresponds to a dissociated O_2 adsorbate, where the O atoms are bridge coordinated to adjacent Pt sites. Nevertheless, for equilibrium interatomic distances, the O_2 molecular orbitals are still defined. Similar calculations[22] without adsorbed O_2 geometry optimization result in a greater contribution of π_z O_2 molecular orbitals which, for a shorter O–O interatomic distance, become closer to the Pt atom just below.

The stabilization of the bridge side-on geometry implies the interaction of the σ and π O atom orbitals with d orbitals in the two closest symmetrically equivalent Pt atoms (Figure 4e,j). This O_2 adsorbate configuration is characterized by the stabilization of the π^* molecular orbitals of O_2 with d_{z^2} Pt atom orbitals. The Mulliken population analysis indicates an oxygen to metal charge transfer without back-bonding. The particular geometry of the Pt site facilitates the simultaneous interactions of both O atoms with adjacent Pt atoms, leading to a greater stabilization of the Pt_NO_2 structure on Pt(100), where the charge transfer is favored because of the lower electronic density of Pt(100) as compared with Pt(111). Despite the similarity of adsorption sites, the local

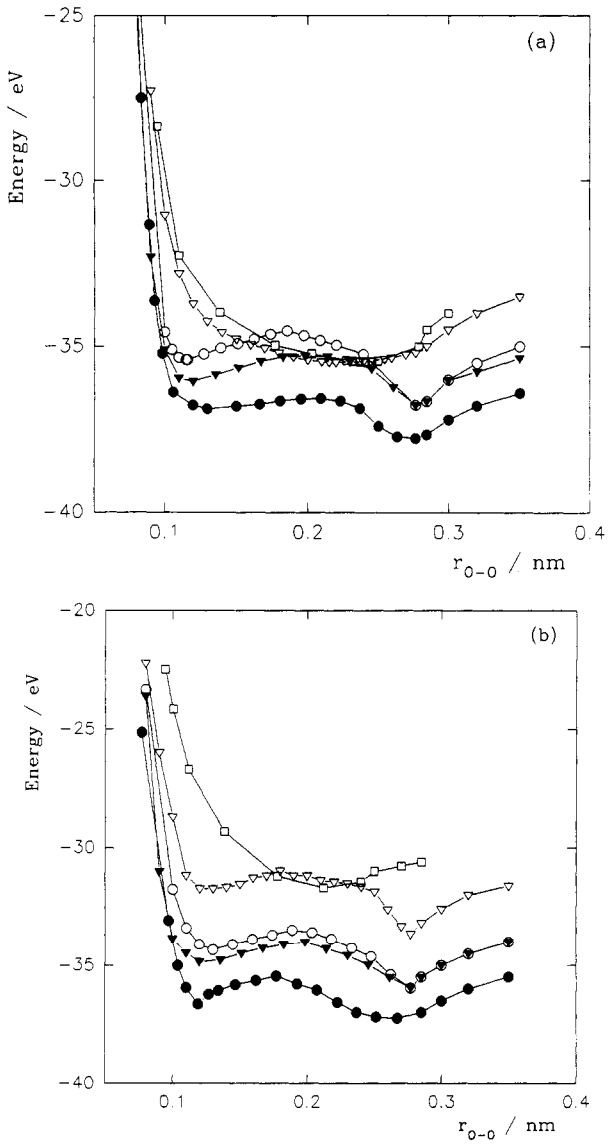

Figure 5. Total energy change (eV) of the Pt_NO_2 ensembles as a function of r_{O-O}. (a) $[Pt(111)]_{18}O_2$, (b) $[Pt(100)]_{18}O_2$. (●) bridge side-on, (○) bridge end-on, (▼) on-top end-on, (▽) hollow, (□) on-top side-on.

geometry, defined by two Pt atoms with $r_{Pt-Pt} = 0.277$ nm on both Pt(100) and Pt(111), leads to an adsorbate geometry with a greater r_{O-O} value on Pt(111). The electronic characteristics of Pt(100) and Pt(111) determine specific charge-transfer contributions and the O_2 molecular orbital occupation. In particular, a greater occupation of O_2 π orbitals on Pt(111) favors (Table 3) larger r_{O-O} values and the O_2 dissociation. Again, as no real local minima can be defined, the adsorbate geometry and electronic characteristics have also been evaluated at the inflection point resulting from the energy vs r_{O-O} plot.

Summing up, data assembled in Table 2 show that the most stable Pt_NO_2 structure corresponds to bridge side-on adsorbate geometry on both Pt(111) and Pt(100), although a larger adsorbate stabilization appears on Pt(100). This difference results from the more efficient overlap of both O atoms with the nearest neighbor Pt atoms on Pt(100). For bridge side-on coordination, the adsorption bond results from a charge transfer from O_2 to the Pt surface and a partial back-bonding to the O_2-π^* orbital. This leads to an increase in r_{O-O} and, then, O_2 dissociation when back-bonding becomes sufficiently large. Negative charge densities in O atoms of the adsorbed O_2 molecule have occasionally been reported,[20,22] especially when no full optimization was considered. Results from this work indicate that the large π^* O_2 population in the O atoms is relaxed when the atomic overlaps are redefined after the geometry optimization routine. On the other hand, the adjustment of the equilibrium potential (VSIP) to minimize the electronegativity difference resulting from Pauling's ionicity relationship results, for this system, in a downward shift of the d band with the simultaneous increase in the VSIP absolute value in O atoms. This means a softening of the back-bonding effect.

Although no experimental data about the $Pt(100)O_2$ adsorbate geometry has been found, NEXAFS measurements of $Pt(111)O_2$[28-31] yielded an $r_{O-O} = 0.132$ nm and a distance of 0.175 nm from the adsorbed O_2 to the first Pt atom layer. These figures agree reasonably well with those resulting from the calculations of this work (Table 2). Furthermore, O–O vibration frequencies of peroxo compounds were detected for the same system by high-resolution EELS spectra (HREELS).[26,27] Likewise, from other semiempirical calculations it has been concluded that σ_{dz^2} and σ_{dzx} orbitals are the most important ones in the stabilization of the adsorption bond.[22] Nevertheless, the molecular orbital analysis made in this work indicates that the interaction between the π O_2 molecular orbitals and d_{xy} Pt atomic orbitals also contributes to the adsorption bonds (Figure 4d,e,i). On the basis of the previous discussion, it has to be emphasized that not the coincidence of our results with those already known for O_2 interaction with Pt(111) but the larger stability of the O_2 molecule on Pt(100) toward dissociation is the main topic of this work.

3.2. Molecular vs Dissociative O_2 Adsorption on Pt. Dissociation of the adsorbed O_2 molecule implies the elongation of the O–O bond until the O–Pt interactions prevail. For the adsorption geometries presented in section 3.1 above, two different adsorbed states can be produced depending on the orientation of the O–O bond relative to the Pt surface. Thus, perpendicular coordination (on-top, bridge, hollow) would result in a single O atom adsorbed on the surface and the second O atom infinitely distant, whereas parallel coordination would lead to a final state of two O atoms coordinated in adjacent positions. The parallel coordination is of particular interest in this work, since O_2 electroreduction first involves a simultaneous H^+ ion and electron transfer prior to dissociation.[6,7] The possibility of O_2 dissociation depends not only on the energy difference between the initial and the final adsorbed states but also on the energy related to the geometry of the intermediates that defines the transition from one to the other.

To analyze the energy associated with the transitions for parallel coordination, r_{O-O} has been varied in 0.005-nm steps from 0.08 to 0.260 nm, and the energy of each ensemble has been evaluated after a full coordinate optimization. The results plotted in Figure 5a,b show a clear stabilization of molecular O_2 for bridge end-on and on-top end-on coordinations. Conversely, O_2 dissociative adsorption appears to be favored for bridge side-on, on-top side-on, and hollow coordinations on both Pt(111) and Pt(100), as the real minima appear for this adsorbed state.

Let us focus our attention on bridge side-on coordination because this structure is associated with the greatest Pt_NO_2 stability and it can also explain the different trends of the O_2 adsorption toward dissociation, depending on the Pt topology.

A clear minimum is defined for $Pt(100)O_2$ with $r_{O-O} = 0.119$ nm and a 0.161-nm value for the perpendicular distance of O_2 to the surface (h in Table 2). Although the energy is lower (0.61 eV) for the dissociated system, an activation energy equal to 0.56 eV is required for the O_2 dissociation on $Pt(100)O_2$. Besides, the lowest energy value is also related to O-atoms bonded to Pt(111), with no other local energy minima except for an inflection in the energy vs r_{O-O} curve. Then, the adsorption of O_2 on Pt(111) involves O_2 dissociation.

The O_2 π^* population is larger on $Pt(111)O_2$ than on $Pt(100)$-O_2 for bridge side-on coordination (Table 3). The filling of antibonding orbitals, which is favored on Pt(111), weakens the O–O bond strength and becomes the main reason why O_2 dissociative adsorption on the most densely packed Pt(111) surface is favored.

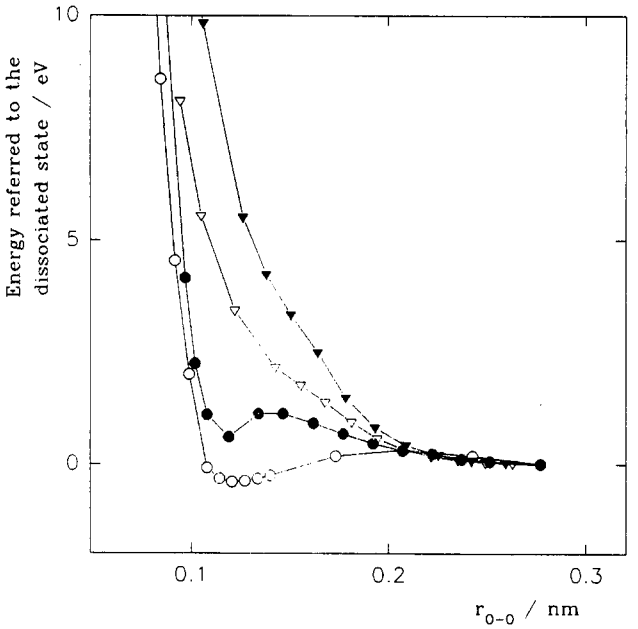

Figure 6. Applied potential dependence of the energy vs r_{O-O} function for the most stable bridge side-on configuration of $[Pt(100)]_{18}O_2$. (▼) −1.4 eV, (▽) −0.8 eV, (●) 0.0 eV, and (○) +0.5 eV. Energy values are normalized to the dissociated state, for each applied potential.

Molecular orbital calculations allow us to conclude that the relative contribution of dissociative and molecular O_2 adsorption on Pt is determined by the relative position of the Pt d band with respect to π^* O_2 orbital energy levels. Because the Pt d band position changes with the applied potential, the characteristics of the O_2 adsorption become potential dependent, as it is expected for the OERR. Thus, positive potentials shift the Pt d band downward, decreasing the π^* O_2 orbital population and favoring molecular adsorption. On the other hand, upward shifting for negatively charged Pt would promote dissociative O_2 adsorption through the filling of the π^* orbitals. The energy vs r_{O-O} plots for bridge side-on adsorption on Pt(100), referred to the dissociated state at different applied potentials (Figure 6), show that no stable molecular O_2 adsorption results on negatively charged surfaces, whereas positive charging results in a $Pt(100)O_2$ ensemble. Similar potential shifts applied to Pt(111) are insufficient to stabilize molecular $Pt(111)O_2$ adsorbate ensembles.

Hence, the influence of the applied electric potential becomes extremely important to determine the stability of O_2 adsorbates on Pt(111) and Pt(100) clusters, which may appear as intermediate surface species in the OERR.

3.3. Possible Species Involved in the Mechanism of OERR on Pt(111) and Pt(100) Surfaces. The preceding structural stability study of O_2 adsorbates on Pt provides the possibility of exploring further mechanistic aspects of the OERR, particularly in relation to possible species involved in the reaction, which may account for the different behavior of Pt(111) and Pt(100) electrode surfaces.

Several mechanisms have been postulated to interpret OERR kinetic data.[12,62-69] Following O_2 dissociative adsorption on Pt(111), the OERR in aqueous acids would imply a possible coordination of H^+ ions from the solution to O adatoms, which further desorb as H_2O at negative potentials. The fact that only H_2O molecules desorb from Pt(111) in the course of the OERR is consistent with the dissociative O_2 adsorption on this Pt surface. In contrast, molecular O_2 adsorption would produce a peroxo-like adsorbate structure on Pt(100) which would give rise to H_2O_2 desorption at negative potentials. Peroxo intermediates and H_2O_2 were experimentally detected mostly on Pt(100) electrodes.[7] Therefore, a tentative explanation for the peroxo intermediate species formation on Pt(100) can be advanced.

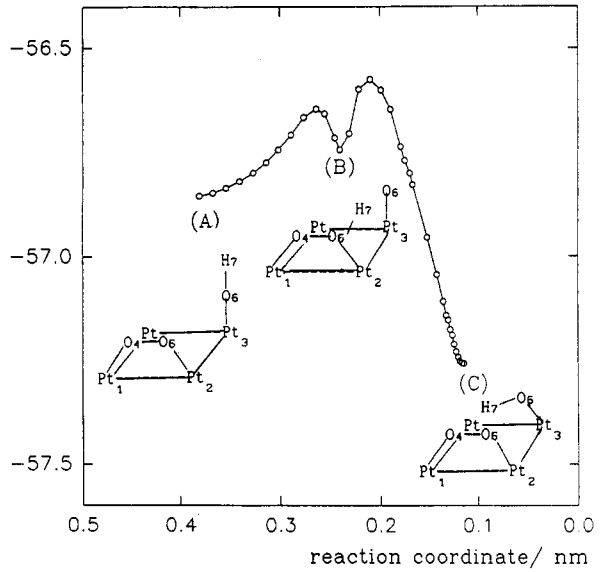

Figure 7. Energies associated with possible steps in the H atom transfer from OH to a peroxo group on $[Pt(100)]_{25}O_2OH$. The arbitrary reaction coordinate is defined as the distance between the H atom and the closest O atom in the peroxo group. (A) Initial state: $r_{O4-O6} = 0.123$ nm, $r_{Pt3-O6} = 0.168$ nm, $r_{O6-H7} = 0.115$ nm, planar angles, $\alpha_{Pt3,O6,H7} = 180°$, $\alpha_{Pt2,Pt3,O6} = 90°$. (B) Intermediate state: $r_{O4-O6} = 0.147$ nm, $r_{Pt3-O6} = 0.182$ nm, $r_{O6-H7} = 0.20$ nm, $\alpha_{Pt3,O6,H7} = 120°$, $\alpha_{Pt2,Pt3,O6} = 80°$. (C) Final state: $r_{O4-O6} = 0.133$ nm, $r_{Pt3-O6} = 0.162$ nm, $r_{O5-H7} = 0.117$ nm, $\alpha_{Pt3,O5,H7} = 151°$, $\alpha_{Pt2,Pt3,O6} = 90°$.

As discussed in section 3.2, peroxo O_2 adsorbates (bridge side-on coordination) would dissociate as the applied potential is shifted negatively (Figure 6) leading to H_2O as the final product as it was also found in Pt(111). However, it should be borne in mind that at potentials where O_2 adsorption on Pt occurs, other species resulting from the H_2O electrochemical and chemical decomposition, such as OH and O adatoms, would also participate in the adsorbate structure, yielding, for instance, a $[Pt(100)]_NO_2$-OH ensemble at the equilibrium potential.

Following the same theoretical procedure, the geometry of the $[Pt(100)]_NO_2OH$ ensemble was fully optimized for both the O_2 and OH adsorbates. The adsorption of OH results in a linear (on-top) configuration adjacent to the peroxo-group bridge side-on adsorbed species, rendering a structure that is 0.84 and 2.04 eV more stable than those associated with an OH bridge and an OH hollow coordination, respectively. Stability calculations of these ensembles showed that a H atom transfer from the hydroxo to the peroxo group is favored. This H atom transfer implies an initial tilting of the Pt–O–H bond until it becomes parallel to the Pt–O bond in the peroxo group, with a simultaneous elongation of the Pt–O bond from 0.168 to 0.182 nm. Besides, the energy increases slightly while the OH bond is bent toward the peroxo group to be finally transferred with a net gain of 0.41 eV in stability (Figure 7). Then, in the OERR potential range, the H atom transfer takes place and the adsorbate ensemble can be better described as a hydrogenated peroxo group plus an O atom coadsorbed on Pt(100). The geometry of this adsorbed ensemble, a possible reaction intermediate in the OERR on Pt(100), has also been fully optimized in bond lengths and angles, as it is shown in Figure 8.

The H atom transfer implies an activation energy equal to 0.26 eV (Figure 7). We are aware that the level of these calculations does not allow us to infer that the proposed intermediate is the one that has the lowest energy. Accordingly, a lower activation energy barrier should not be precluded. The energy required for the $Pt(100)O_2OH$ to $Pt(100)O_2HO$ transition might be provided by other simultaneous reactions, such as the underpotential deposition, upd, H_2O discharge, or the O_2 adsorption on Pt.

The stability of the O_2H–O coadsorbate on Pt(100) was also calculated as a function of the applied potential. Changes in the

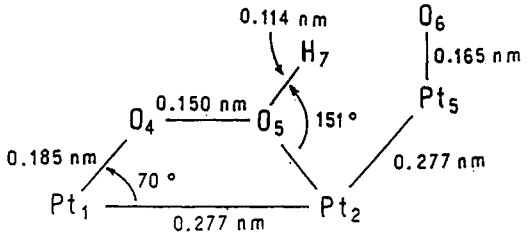

Figure 8. Geometric parameters of the fully optimized adsorbed ensemble structure, resulting from $[Pt(100)]_{25}O_2OH$, after the H atom transfer from OH to a peroxo group.

TABLE 4: Charges on Pt and O_2 (q_{Pt} and q_O) and Mulliken Overlap Populations (c_i) for Relevant Bonds at the $[Pt(100)]_{25}O_2OH$ Ensemble at Different Potentials (E)

	E (eV)				
	0.0	−0.40	−0.80	−1.00	−1.40
q_{Pt1} (eu)	1.4215	1.3536	1.3382	1.3372	1.2926
q_{Pt2}(eu)	1.3980	1.3620	1.3425	1.3176	1.3174
q_{Pt3} (eu)	2.1640	2.3447	2.3281	2.2463	2.0765
q_{O4} (eu)	0.6435	0.0125	−0.2663	−0.3754	−0.5477
q_{O5} (eu)	1.0642	0.6393	0.4077	0.3224	0.1854
q_{O6} (eu)	0.6435	0.2380	−0.2964	−0.5522	−0.9173
q_{H7} (eu)	0.2226	0.2107	0.2004	0.1956	0.1879
c_{Pt1-O4}	0.7447	0.6731	0.6006	0.6335	0.6108
c_{Pt2-O5}	0.6705	0.6313	0.5440	0.6038	0.5882
c_{O4-O5}	0.3563	0.3084	0.3226	0.2739	0.2496
c_{O5-H7}	0.4647	0.4691	0.5507	0.4741	0.4764
c_{Pt3-O6}	1.2255	1.1814	0.6501	0.9994	0.8771

adsorbed structure due to the upward shifting of the d band, *i.e.*, potential negatively increased, have been studied, after a full optimization of the geometry for each set of the defined conditions. Thus, the activation energy barrier for the H atom displacement from oxygen 6 to oxygen 5 (Figure 8) depends on the potential, and it decreases almost to zero for a −1 eV potential assisting the OERR in the forward direction. Accordingly, it is reasonable to admit that the larger the cathodic overpotential the lower the activation energy.

Changes in the Mulliken atomic overlaps with the applied potential (Table 4) show that, although they both decrease for negative potentials, the destabilization of the Pt–O bond becomes more pronounced than that of the O–O bond for a given potential change. Hence, although a competition between the dissociation of the peroxo adsorbate and the formation of a hydroperoxo intermediate ensemble takes place, it is likely that the hydroperoxo intermediate ensemble preferentially desorbs as H_2O_2 prior to dissociation. On the other hand, negative applied potentials stabilize the large negative charge density in the O atom at the peroxo group not bonded to H atom (oxygen 4 in Figure 8) which becomes a center for the H^+ ion coordination, followed by H_2O_2 desorptive formation.

The hydroperoxide formation on Pt(100) implies that at negative potentials, the remaining oxo species (Figure 7) would be negatively charged (Table 4) and, after the H^+ ion coordination, H_2O desorption would occur. The mechanism for this reaction is similar to that proposed on Pt(111), and it justifies the simultaneous desorption of H_2O from Pt(100) and the detection of H_2O as the only OERR product on Pt(111).

4. Conclusions

The interaction of a single O_2 molecule on Pt(111) and Pt(100) structures was studied. On both surfaces, bridge side-on is the most stable coordination geometry for Pt_NO_2. However, a dissociative O_2 interaction on Pt(111) and a molecular O_2 interaction on Pt(100) are favored. The different characteristics of the O_2 adsorption on both surfaces are reflected in the OERR, leading to the preferential desorption of H_2O from Pt(111) and H_2O_2 from Pt(100).

H_2O desorption results from the coordination of H^+ ions from the media to O adatoms in the adsorbate ensemble, which become negatively charged for negative applied potentials due to the upward shift of the Pt d band. On the other hand, H_2O_2 results from the coordination of an H^+ ion to peroxo intermediates adsorbed on Pt(100), which are more likely to desorb than to dissociate, according to the larger decrease in the Pt–O than the O–O overlaps, at negative potentials.

Results from this quantum chemical approach justify the detection of peroxo and oxo intermediates on Pt(100) structures in the course of the OERR, rather than the structure of the oxo intermediates on Pt(111).

Acknowledgment. This work was financially supported by the Consejo Nacional de Investigaciones Cientfficas y Técnicas (CONICET) and Fundación Antorchas of Argentina. C.F.Z. thanks the Universidad de la República, Montevideo (Uruguay), for the fellowship granted.

References and Notes

(1) Tarasevich, M. R.; Sadkowski, A.; Yeager, E. B. Oxygen Electrochemistry. In *Comprehensive Treatise of Electrochemistry, Vol. 7: Kinetics and Mechanisms of Electrode Processes*; Conway, B. E., Bockris, J. O'M., Yeager, E. B., Kahn, S., White, R. W., Eds.; Plenum Press: New York, 1983; Chapter 6, pp 301–398.
(2) Hoare, J. P. *The Electrochemistry of Oxygen*; J. Wiley and Sons: New York, 1968.
(3) Appleby, A. J. *In Modern Aspects of Electrochemistry*; Bockris, J. O'M., Conway, B. E., Eds.; Plenum Press: New York, 1974; Vol. 9, Chapter 5.
(4) Damjanovic, A.; Brusic, V. *Electrochim. Acta* **1967**, *12*, 615.
(5) Huang, J. C.; Sen, R. K.; Yeager, E. B. *J. Electrochem. Soc.* **1979**, *126*, 736.
(6) Yeager, E. B. *Electrochim. Acta* **1984**, *29*, 1527.
(7) Zinola, C. F.; Castro Luna, A. M.; Triaca, W. E.; Arvia, A. J. *J. Appl. Electrochem.* **1994**, *24*, 119.
(8) El Kadiri, F.; Faure, R.; Durand, R. *J. Electroanal. Chem.* **1991**, *301*, 777.
(9) Zinola, C. F.; Castro Luna, A. M.; Triaca, W. E.; Arvia, A. J. *J. Appl. Electrochem.*, in press.
(10) (a) Appleby, A. J. *J. Electroanal. Chem.* **1970**, *24*, 97. (b) Parthasarathy, A.; Srinivasan, S.; Appleby, J.; Martin, C. R. *J. Electroanal. Chem.* **1992**, *339*, 101. (c) Parthasarathy, A.; Srinivasan, S.; Appleby, J.; Martin, C. R. *J. Electrochem. Soc.* **1992**, *139*, 2856. (d) Parthasarathy, A.; Srinivasan, S.; Appleby, J.; Martin, C. R. *J. Electrochem. Soc.* **1991**, *138*, 916.
(11) Hsueh, K.-L.; González, E.; Srinivasan, S.; Chin, D.-T. *J. Electrochem. Soc.* **1984**, *131*, 822.
(12) Damjanovic, A.; Genshaw, M. A.; Bockris, J. O'M. *J. Chem. Phys.* **1964**, *45*, 4057.
(13) Ross, P. N.; Andriacos, P. C. *J. Electroanal. Chem.* **1983**, *154*, 205.
(14) Glass, J. T.; Cahen, G. L., Jr.; Stoner, G. E. *J. Electrochem. Soc.* **1989**, *136*, 656.
(15) Guo, X.-C.; Bradley, J. M.; Hopkins, A.; King, D. A.; *Surf. Sci. Lett.* **1993**, *292*, L786.
(16) Poehlmann, E.; Schmitt, M.; Hoinkes, H.; Wilsch, H. *Surf. Sci.* **1993**, *291*, 317.
(17) de Meijere, A.; Hiriyama, H.; Hasselbrink, E. *Phys. Rev. Lett.* **1993**, *70*, 1147.
(18) Ohno, Y.; Matsushima, T.; Tanaka, S.; Yagasaki, E.; Kamada, M. *Surf. Sci.* **1992**, *275*, 281.
(19) Benesh, G. A.; Lingane, L. S. G. *Surf. Sci.* **1992**, *261*, 207.
(20) Hellsing, B. *Surf. Sci.* **1993**, *282*, 216.
(21) Nakatsuji, H.; Nakai, H. *J. Chem. Phys.* **1993**, *98*, 2423.
(22) Chan, A. W. E.; Hoffmann, R.; Ho, W. *Langmuir* **1992**, *8*, 1111.
(23) Panas, I.; Sieghbahn, P. *Chem. Phys. Lett.* **1988**, *88*, 458.
(24) Selmani, A.; Andzelm, J.; Salahub, D. R. *Int. J. Quantum Chem.* **1986**, *29*, 829.
(25) Barteau, M. A.; Ko, E. I.; Maddix, R. J. *Surf. Sci.* **1981**, *102*, 99.
(26) Steininger, H.; Lehwald, S.; Ibach, H. *Surf. Sci.* **1982**, *123*, 1.
(27) Vaska, L. *Acc. Chem. Res.* **1976**, *9*, 175.
(28) Outka, D. A.; Stöhr, J.; Jark, W. *Phys. Rev. B* **1987**, *35*, 4119.
(29) Wurth, W.; Stöhr, J.; Feulner, P.; Pan, X.; Bauchspiess, K. R.; Baba, Y.; Hudel, E.; Rocker, G.; Mentzel, D. *Phys. Rev. Lett.* **1990**, *65*, 2426.
(30) Stöhr, J.; Gland, J. L.; Eberhardt, W.; Outka, D.; Madix, R. J.; Sette, F.; Koestner, R. J.; Doebler, U. *Phys. Rev. Lett.* **1983**, *51*, 2414.
(31) Sexton, B.; Madix, R. J. *Chem. Phys. Lett.* **1980**, *76*, 294.
(32) Gland, J. L.; Sexton, B.; Fisher, G. B. *Surf. Sci.* **1980**, *95*, 587.
(33) Nakatsuji, H.; Nakai, H.; Hada, M. *Metal-Ligand Interactions: from Atoms, to Clusters, to Surfaces*; Salahub, D. R., Russo, N., Eds.; Kluwer Academic Publishers: Dordrecht, 1992; pp 251–285.
(34) Przybylski, K.; Koutecky, J.; Bonačic-Koutecky, V.; Schleyer, P. v. R.; Guest, M. F. *J. Chem. Phys.* **1991**, *94*, 5533.

(35) Goursot, A.; Papai, I.; Salahub, D. R. *J. Am. Chem. Soc.* **1992**, *114*, 7452.
(36) Bagus, P. S.; Pacchioni, G. *Surf. Sci.* **1990**, *236*, 233.
(37) Hoffmann, R. *J. Chem. Phys.* **1963**, *39*, 1397.
(38) Anderson, A. B.; Hoffmann, R. *J. Phys. Chem.* **1974**, *60*, 4271.
(39) Anderson, A. B. *J. Phys. Chem.* **1975**, *62*, 1187.
(40) (a) Head, J. D.; Zerner, M. C. *Chem. Phys. Lett.* **1985**, *122*, 264. (b) Head, J. D.; Zerner, M. C. *Chem. Phys. Lett.* **1986**, *131*, 359.
(41) Anders, L. W.; Hansen, R. S.; Bartell, L. S. *J. Chem. Phys.* **1973**, *59*, 5277.
(42) Calzaferri, G.; Forss, L.; Kamber, I. *J. Phys. Chem.* **1989**, *93*, 5366.
(43) Savary, F.; Weber, J.; Calzaferri, G. *J. Phys. Chem.* **1993**, *97*, 3722.
(44) Calzaferri, G.; Hoffmann, R. *J. Chem. Soc., Dalton Trans.* **1991**, 917.
(45) Amouyal, E.; Mouallem-Bahout, M.; Calzaferri, G. *J. Chem. Phys.* **1991**, *95*, 7641.
(46) Brändle, M.; Calzaferri, G. *Helv. Chim. Acta* **1993**, *76*, 924.
(47) (a) Vázquez, L.; Gómez Rodríguez, J. M.; Gómez Herrero, J.; Baró, A. M.; García, N.; Canullo, J. C.; Arvia, A. J. *Surf. Sci.* **1987**, *181*, 98. (b) Gómez, J.; Vázquez, L.; Baró, A. M.; García, N.; Perdriell, C. L.; Triaca, W. E.; Arvia, A. J. *Nature* **1986**, *323*, 612. (c) Cerviño, R. M.; Arvia, A. J.; Vielstich, W. E. *Surf. Sci.* **1985**, *154*, 623.
(48) Tarasevich, M. R. *Elektrokhimiya* **1973**, *9*, 599.
(49) Vilinskaya, V. S.; Tarasevich, M. R. *Elektrokhimiya* **1973**, *8*, 1187.
(50) Villambi, N. R. K.; Taylor, E. J. *Electrochim. Acta* **1989**, *34*, 1449.
(51) Park, S.-M.; Ho, S.; Aruliah, S.; Weber, M. F.; Ward, C. A.; Venter, R. D.; Srinivasan, S. *J. Electrochem. Soc.* **1986**, *133*, 1641.
(52) Anastasijevic, N. A.; Vesovic, V.; Adžic, R. R. *J. Electroanal. Chem.* **1987**, *229*, 305.
(53) Pauling, L. *The Nature of the Chemical Bond*, 3rd ed.; Cornell University Press: Ithaca, NY, 1992, p 45.
(54) Calzaferri, G.; Brändle, M. QCMP *116*. *QCPE Bull* **1992**, *12*, No. 4.
(55) Estiú, G. L.; Maluendes, S. A.; Castro, E. A.; Arvia, A. J. *J. Electroanal. Chem.* **1990**, *284*, 289.
(56) Estiú, G. L.; Maluendes, S. A.; Castro, E. A.; Arvia, A. J. *J. Phys. Chem.* **1988**, *92*, 2512.
(57) Lide, D. R., Ed. *CRC Handbook of Chemistry and Physics*; CRC Press: Boca Raton, FL, 1990–91.
(58) Levine, I. N. *Quantum Chemistry*; Editorial A.C.: Madrid, 1977.
(59) Taube, H. *J. Gen. Phys.* **1965**, *49*, 29.
(60) Greenwood, N. N.; Earnshaw, A. In *Chemistry of the Elements*; Pergamon Press: Oxford, 1984.
(61) Calzaferri, G.; Marcolli, C. To be published.
(62) Anastasijevic, N. A.; Vesovic, V.; Adžic, R. R. *J. Electroanal. Chem.* **1987**, *229*, 317.
(63) Zurilla, R. W.; Yeager, E. B. *Technical Report No. 23*, Case Western University, 1969.
(64) Wroblowa, H. S.; Pan, Y-Chi; Razumney, G. *J. Electroanal. Chem.* **1976**, *69*, 195.
(65) Bagotskii, V. S.; Tarasevich, M. R.; Filinovskii, V. Yo; *Elektrokhimiya* **1969**, *5*, 1218.
(66) Bagotskii, V. S.; Tarasevich, M. R.; Filinovskii, V. Yo; *Elektrokhimiya* **1972**, *6*, 84.
(67) Hsueh, K. L.; Chin, D. T.; Srinivasan, S. *J. Electroanal. Chem.* **1983**, *153*, 79.
(68) O'Grady, W. E.; Taylor, E. J.; Srinivasan, S. *J. Electroanal. Chem.* **1982**, *132*, 137.
(69) Gnanamuthu, D. S.; Petrocelli, V. J. *J. Electrochem. Soc.* **1971**, *114*, 1036.